RSC Advances

PAPER

View Article Online
View Journal | View Issue

Cite this: *RSC Adv.*, 2021, **11**, 23064

Flower-like MoS_2 microspheres compounded with irregular CdS pyramid heterojunctions: highly efficient and stable photocatalysts for hydrogen production from water

Kai He [a] and Liejin Guo*[b]

An irregular CdS pyramid/flower-like MoS_2 microsphere composite photocatalyst was successfully synthesized using a simple one-step hydrothermal method. The as-prepared samples were characterized by X-ray diffraction, X-ray photoelectron spectroscopy, scanning electron microscopy, ultraviolet visible absorption spectroscopy, fluorescence spectroscopy and photoelectrochemical tests. The composite photocatalysts showed superior photocatalytic activities for hydrogen evolution from water under visible light irradiation ($\lambda \geq 420$ nm) with an extremely high apparent quantum yield (AQY = 64.8%) at 420 nm. To our knowledge, this value is the highest reported efficiency value for CdS/MoS_2 photocatalysts. Further detailed characterization revealed that the special structure for some CdS pyramid structures dispersed in the MoS_2 microsphere structures and surrounded by MoS_2 nanosheets led to the photogenerated electrons migrating from the conduction band of different faces of the CdS pyramid to the conduction band of different MoS_2 nanosheets while photogenerated holes remained in the CdS pyramid structures, which greatly promoted the separation of photogenerated electrons and holes, improving the photoactivity of the CdS/MoS_2 catalyst. The catalyst also exhibited perfect stability, and the photoactivity displayed no significant degradation during continuous hydrogen production over nearly 70 h.

Received 17th May 2021
Accepted 23rd June 2021

DOI: 10.1039/d1ra03834f

rsc.li/rsc-advances

1. Introduction

Hydrogen is a type of clean and nonpolluting renewable energy that has attracted great interest and has the potential to solve the global energy crisis and reduce environmental pollution. An ideal approach for preparing hydrogen using solar energy to generate photocatalytic water splitting could convert solar energy to clean and storable hydrogen energy. The key issue to achieve hydrogen production from solar photocatalytic water splitting is to develop semiconductor catalysts with high activity and stability.[1–8] Among many different kinds of photocatalysts, sulfide photocatalysts have more matching band gaps and higher visible light absorption efficiencies for hydrogen production, which have attracted much attention and have shown potential in industrial applications.[9–17] CdS, in particular, is the most widely studied sulfide photocatalyst because of its small band gap (approximately 2.3 eV).[14] Moreover, CdS loaded by some noble metals, including Pt, Pd, Ru and so on, showed a much higher photogenerated charge efficiency, which greatly improved the CdS photocatalytic hydrogen production activity.[18–20] CdS loaded with 0.3 wt% Pt and 0.13 wt% PdS exhibited the best photocatalytic hydrogen production activity with an apparent quantum yield of 64.8% at 420 nm.[18,19] However, considering the cost, some inexpensive metals and compounds as cocatalysts have attracted increasing interest.[21–25] Investigations have indicated that MoS_2-loaded CdS photocatalysts can also realize high photocatalytic activity.

Many highly active MoS_2-loaded CdS photocatalysts have been reported in the literature.[26–43] Zhao *et al.* reported a platinum-free 1D/2D CdS/MoS_2 photocatalyst, and their experimental results showed that the highest hydrogen production rate of 1.79 mmol g^{-1} h^{-1} was obtained when the reaction ratio of CdS to MoS_2 was 0.3.[41] Yin *et al.* reported noble-metal-free CdS@MoS_2 core–shell nanoheterostructures. 6 wt% MoS_2-loaded CdS exhibited the best photocatalytic H_2 evolution performance thus far, with a rate of 62.55 mmol g^{-1} h^{-1}.[34] Jiang *et al.* reported a berry-shaped (b)-CdS/MoS_2 photocatalyst, and 1 wt% MoS_2-loaded CdS exhibited the best photocatalytic H_2 evolution performance thus far, with a rate of 63.59 mmol g^{-1} h^{-1}.[40] Reddy *et al.* successfully synthesized a few-layered black phosphorus/MoS_2 nanohybrid as a promising cocatalyst, 8 wt% of which loaded on CdS nanorods showed a much higher hydrogen production rate of 183.24 mmol g^{-1} h^{-1}.[35] Ultrasmall

[a]*School of Mechanical Engineering, Shaanxi University of Technology, Hanzhong 723000, China*

[b]*International Research Centre for Renewable Energy, State Key Laboratory of Multiphase Flow in Power Engineering, Xi'an Jiaotong University, Shaanxi 710049, China. E-mail: lj-guo@mail.xjtu.edu.cn; Fax: +86 29 82669033; Tel: +86 29 82663895*

cobalt nanocrystals embedded in 2D-MoS_2 nanosheets as efficient cocatalysts for solar-driven hydrogen production were reported by Lee *et al.* Thus, a Co–MoS_2 cocatalyst loaded on CdS nanorods showed a very high H_2 production rate (275 mmol g^{-1} h^{-1}) when the mass fraction of MoS_2 loaded with 1 wt% Co was 6%, which was the most active MoS_2-loaded CdS photocatalyst for hydrogen production reported in the literature.[33]

Through analysis of the abovementioned literature, only a small amount of MoS_2 loaded on CdS exhibited a high photocatalytic activity for hydrogen production. Here, we report a kind of MoS_2/CdS photocatalyst with flower-like MoS_2 microspheres compounded with irregular CdS pyramids. The special structures led to the CdS/MoS_2 photocatalyst exhibiting a superior separation efficiency for photogenerated electrons and holes. When the molar ratio of MoS_2 to CdS was 1 : 1, the MoS_2/CdS photocatalyst showed the highest hydrogen production rate of 394 mmol g^{-1} h^{-1}, and the apparent quantum yield reached 64.8% at 420 nm. To our knowledge, this value is the highest efficiency ever reported for MoS_2-modified CdS photocatalysts.

2. Experimental

2.1. Synthesis

All chemicals were of analytical grade and were used as received without any further purification. Cadmium acetate ($Cd(CH_3COO)_2 \cdot 2H_2O$), ammonium molybdate ($(NH_4)_6Mo_7O_{24} \cdot 4H_2O$), thiourea ($CH_4N_2S$), and ethanol ($C_2H_6O$) were purchased from Sino-pharm Chemical Reagent of China.

Five proper amounts of ammonium molybdate (the molar of 0.01, 0.0071, 0.005, 0.0042 and 0.0033 mol) were dissolved in deionized water (70 mL) in Teflon tubes (100 mL), and then, appropriate amounts of $Cd(CH_3COO)_2 \cdot 2H_2O$ (the molar ratios of Cd to Mo were 0.5, 0.7, 1, 1.2 and 1.5) and excessive thiourea were added to the solution, with stirring for several minutes. The Teflon tubes were transferred to autoclaves, which were sealed and heated at 200 °C for 24 h. The resulting precipitates collected by centrifugal separation were washed with deionized water and absolute ethanol several times and then dried under vacuum for 24 h at 80 °C. The catalysts prepared by this method were denoted as CdS/

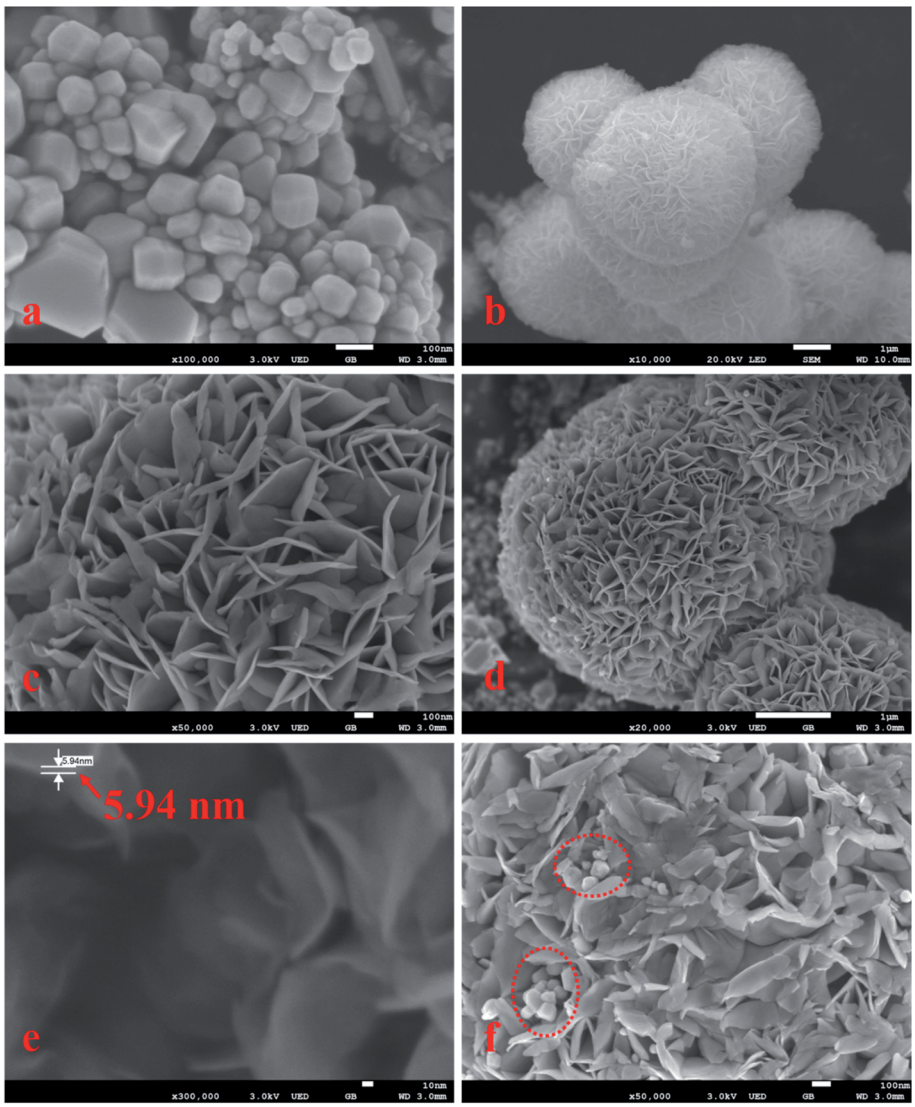

Fig. 1 SEM images of CdS/MoS_2 (a–f).

MoS_2-*i* (molar ratios of Cd to Mo, $i = 0.5$, 0.7, 1, 1.2 and 1.5). "CdS/MoS_2" was "CdS/MoS_2-1" in "3. Results and discussion".

Pure CdS and MoS_2 were also prepared using the same process described above.

Based on CdS/MoS_2-1, a Pt-loaded CdS/MoS_2-1 catalyst was prepared by an *in situ* photoreduction method using a Xe lamp (300 W) equipped with a 420 nm cutoff filter, as follows: a certain amount of CdS/MoS_2-1 was added to a 200 mL aqueous solution containing 10 vol% lactic acid and 0.25 M Na_2SO_3/0.35 M Na_2S. A certain amount of chloroplatinic acid (2 wt% of the CdS/MoS_2-1 quality) was added to the two aqueous solutions. Then, the Pt-loaded CdS/MoS_2-1 catalyst was obtained after the aqueous solution was photoreduced for 1 h, denoted as Pt/CdS/MoS_2-1.

Pure CdS and MoS_2 were mechanically mixed, and then a Pt-loaded catalyst was prepared by the same method, denoted as Pt/CdS + MoS_2.

2.2. Characterization

The X-ray diffraction (XRD) patterns of the as-prepared photocatalysts were obtained on a PANalytical X'pert MPD Pro X-ray diffractometer equipped using Cu-Kα irradiation. Scanning electron microscopy (SEM) images were obtained using a JSM-7800F-type field emission scanning electron microscope. X-ray photoelectron spectroscopy (XPS) measurements were obtained on an Axis Ultra Kratos (UK) multifunctional spectrometer with monochromatic Al Kα radiation. The ultraviolet visible (UV-vis) absorption spectra were measured on a HITACHI U-4100 spectrophotometer. Fluorescence spectroscopy was performed using a PTI QM-4 fluorescence spectrophotometer.

2.3. Photocatalytic hydrogen production

Photocatalytic reactions for hydrogen production were performed in a side irradiation Pyrex cell. A total of 0.01 g of catalyst powder (CdS/MoS_2-*i*, Pt/CdS/MoS_2–I or Pt/CdS + MoS_2) was added to an aqueous solution (200 mL) containing 10 vol% lactate acid or 0.35 M Na_2S/0.25 M Na_2SO_3 as electron donors. Nitrogen was purged in the cell to remove oxygen before irradiation. The solution was irradiated by visible light through a Xe lamp (300 W) equipped with a 420 nm cutoff filter. The amount of hydrogen was determined using TCD gas chromatography

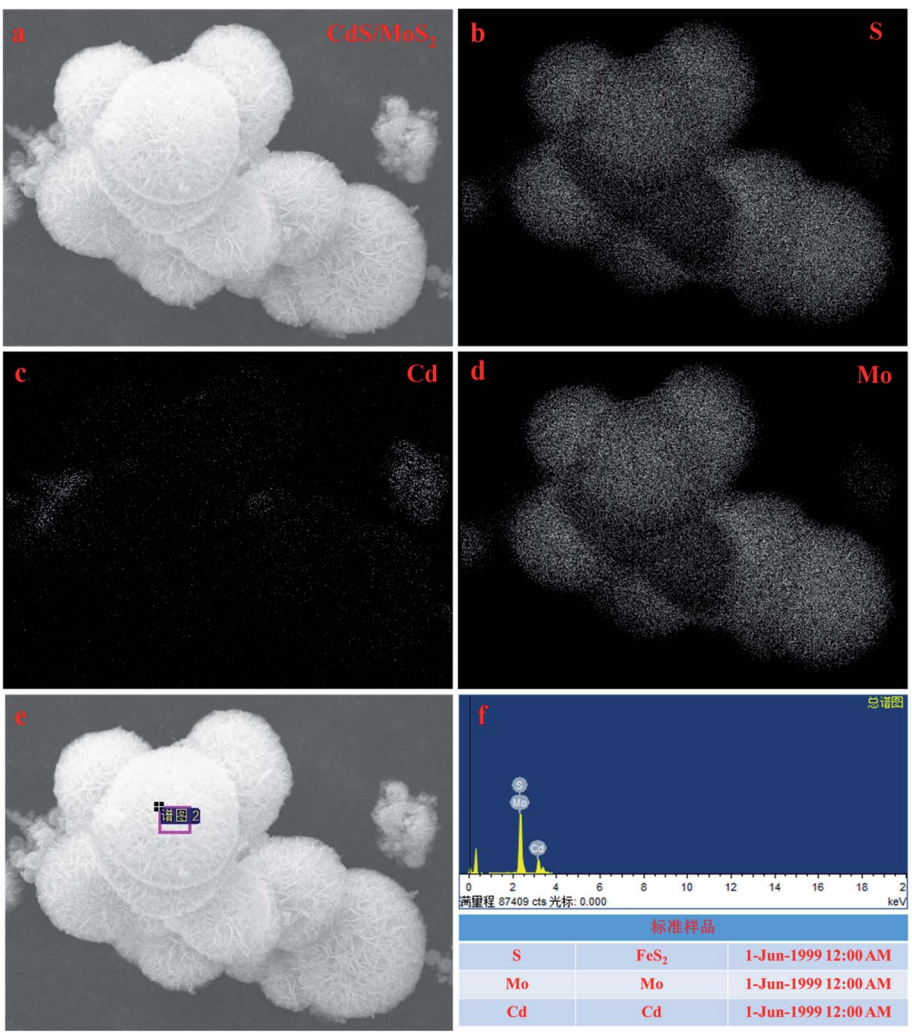

Fig. 2 SEM image of CdS/MoS_2 (a) and SEM mapping images of S, Cd and Mo (b–f).

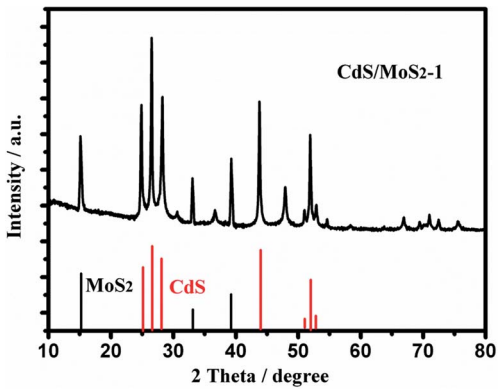

Fig. 3 XRD patterns of CdS/MoS_2.

(NaX zeolite column, TCD detector, N_2 as carrier gas). The apparent quantum yield (AQY) was calculated according to the equation reported in the literature.[11]

3. Results and discussion

Fig. 1 shows SEM images of the samples. As shown in the images (Fig. 1a and b), the morphology of the samples presented differently sized irregular pyramid structures with particle sizes of 10–300 nm (Fig. 1a) and flower-like microspheres with particle sizes of 4–7 μm (Fig. 1b). The flower-like microsphere structures were self-assembled by a plurality of nanosheets with a thickness of 5.94 nm (Fig. 1c–e). Some irregular pyramid structures were surrounded by nanosheets with microsphere structures, and different surfaces of irregular pyramid structures directly contacted nanosheets, as shown in Fig. 1f. The irregular pyramid structures and flower-like microspheres were presumed to be CdS and MoS_2, and in addition, some CdS pyramid structures were dispersed in the MoS_2 microsphere structures.

To further prove the above inferred conclusion, SEM mapping of the CdS/MoS_2 catalyst was performed, as shown in Fig. 2. As seen, S was distributed throughout the entire catalyst region (Fig. 2b), demonstrating that Mo and Cd were in the form of MoS_2 and CdS in the catalyst. The distribution of Mo (Fig. 2d) was more intensive in the distribution region of the microsphere structures (Fig. 2a), illustrating that MoS_2 formed microsphere structures in the catalyst. The content of Cd was very low, as shown in Fig. 2c, and was distributed in the MoS_2 microsphere structures (Fig. 3c). Some box samples in Fig. 2c were used for element analysis, and the results are shown in Table 1. It can be seen from the table that the microsphere structure was MoS_2, and a small amount of CdS pyramid structures was dispersed in the MoS_2 microsphere structure.

Table 1 Local element composition of CdS/MoS_2

Element	Element concentration	Intensity correction	Weight percent	Weight percent sigma	Atom percent
S K	14.03	1.0538	29.61	0.34	57.93
Mo L	12.16	0.9325	29.00	0.60	18.96
Cd L	12.55	0.6741	41.39	0.42	23.10
Total			100.00		

Fig. 3 shows the XRD patterns of CdS/MoS_2-1. As shown from the patterns, the diffraction peaks of the hexagonal phase CdS (JCPDF no. 41-1049) appeared at 25°, 26°, 28°, 51°, 52° and 53°, and the diffraction peaks of cubic phase CdS (JCPDF no. 45-0647) appeared at 26°, 31°, 37°, 44°, 48° and 52°. The diffraction peaks of hexagonal phase MoS_2 (JCPDF no. 75-1539) appeared at 15.1°, 34.2° and 39.5°. Compared with pure CdS and MoS_2, the diffraction peaks of CdS/MoS_2-1 showed no movement with the addition of MoS_2 or CdS, which revealed that MoS_2 and CdS only contacted the surface instead of being absorbed into each other's lattice.

Fig. 4 shows the UV-vis absorption spectra of pure CdS, pure MoS_2 and CdS/MoS_2-1. Pure MoS_2 had absorption over the whole wavelength range of 400–800 nm, while the absorption edge of pure CdS was located at 536 nm. The band gaps of pristine CdS and MoS_2 were estimated to be 2.31 eV and 1.32 eV, respectively, by the Kubelka–Munk function.[11] CdS/MoS_2-1 showed an apparent enhancement of the visible light absorption from 536 to 800 nm, which was attributed to the absorption of MoS_2 over the entire wavelength range of 400–800 nm. It was revealed that the narrow band gap of MoS_2 could improve the visible absorption of CdS/MoS_2 heterojunctions. The enhanced light absorption of the catalysts was expected to favor the formation of more photogenerated electrons available for photocatalytic hydrogen production.

The peaks of Cd, Mo and S electrons in the XPS survey scan spectra of CdS/MoS_2 shown in Fig. 5a were identified for the samples, confirming the successful synthesis of CdS/MoS_2. Fig. 5b–d show high-resolution XPS spectra of S 2p, Cd 3d and Mo 3d for pure CdS, MoS_2 and CdS/MoS_2, respectively. Compared to pure CdS and MoS_2, the absorption peaks of Cd 3d and S 2p for CdS/MoS_2 were redshifted by 0.4 eV and 0.2 eV, while the absorption peaks of Mo 3d and S 2p for CdS/MoS_2 were blueshifted by 0.3 eV and 0.2 eV, respectively, which were mainly derived from the electronic interaction between CdS and MoS_2. The redshift and blueshift revealed that the density of

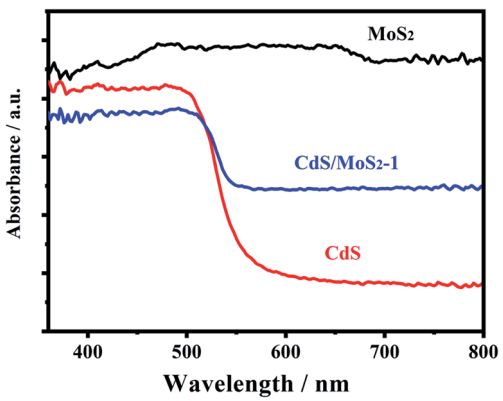

Fig. 4 Uv-vis absorption spectra of pure CdS, pure MoS_2 and CdS/MoS_2-1.

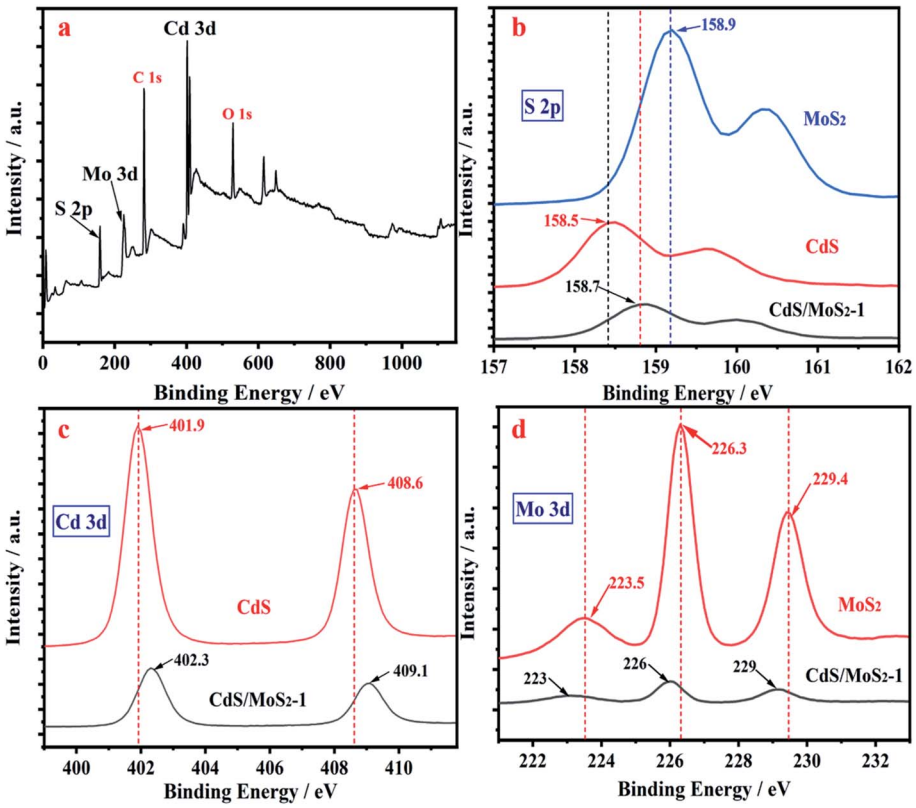

Fig. 5 XPS spectra of CdS/MoS_2 (a); high-resolution XPS spectra of S 2p (b); high-resolution XPS spectra of Cd 3d (c) and of Mo 3d (d) for pure CdS, MoS_2 and CdS/MoS_2.

electrons in CdS decreased and that in MoS_2 increased, resulting in an increase and decrease in the binding energy for CdS and MoS_2, respectively; thus, it was inferred that photoelectrons transferred from CdS to MoS_2, which achieved efficient separation of photogenerated charges between CdS and MoS_2, improving the photocatalytic activity for hydrogen production.

The photoluminescence spectra of pure CdS and CdS/MoS_2 were also measured and are shown in Fig. 6. The spectra present emission peaks at 475–550 nm, which were related to the recombination process of electrons and holes in the semiconductor. Compared with pure CdS, the CdS/MoS_2 peak showed a much lower intensity, revealing that CdS/MoS_2 exhibited a superior efficiency of separation for photogenerated electrons and holes, which improved the photocatalytic activity for hydrogen production.

Photocurrent experiments were also performed to further illustrate the charge transfer behavior for CdS/MoS_2-1 and pure CdS, as shown in Fig. 7. The photoelectrodes for photoelectrochemical test samples were prepared by electrophoretic

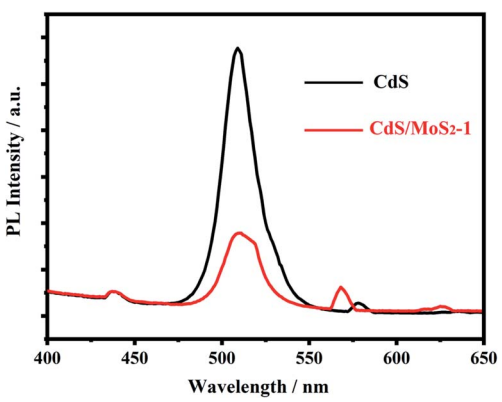

Fig. 6 Photoluminescence spectra of pure CdS and CdS/MoS_2, excitation 370 nm.

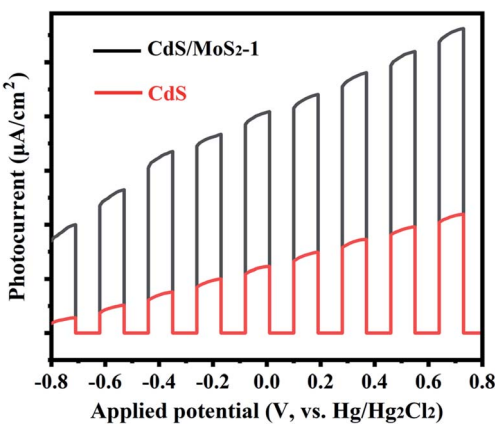

Fig. 7 The current–potential characteristics of as-prepared pure CdS and CdS/MoS_2-1. Test condition: A 300 W Xe lamp coupled with an AM 1.5 filter was used as the light source; photocurrent density was measured in the 0.5 M Na_2SO_3 aqueous solution as the electrolyte; Hg/Hg_2Cl_2 was as the reference electrode.

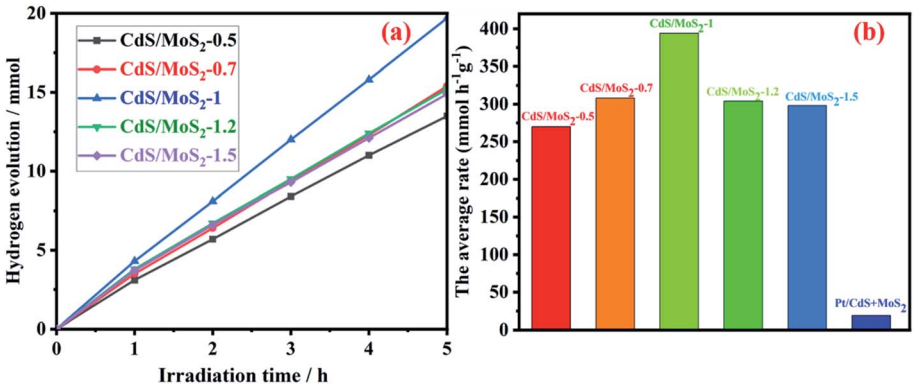

Fig. 8 Photocatalytic hydrogen production activities of CdS/MoS_2-*i* (the molar ratio of Cd to Mo, $i = 0.5$, 0.7, 1, 1.2 and 1.5) and Pt/CdS + MoS_2. Reaction condition: 0.01 g of catalyst; 200 mL of aqueous solution containing 180 mL deionized water and 20 mL lactate acid; 300 W Xe lamp equipped with a cutoff filter ($\lambda > 420$ nm).

deposition (EPD) onto fluorine-doped tin oxide (FTO)-coated glass substrates. As shown in Fig. 7, the photocurrent density of the samples increased gradually with increasing applied potential. Compared with pure CdS, CdS/MoS_2-1 exhibited an extremely higher photocurrent density, indicating that CdS/MoS_2-1 showed more efficient charge separation than pure CdS, which improved the photocatalytic activity for hydrogen production.

The amount and average rate of photocatalytic hydrogen production during 5 h irradiation for CdS/MoS_2-*i* (molar ratios of Cd to Mo, $i = 0.5$, 0.7, 1, 1.2 and 1.5) are shown in Fig. 8. With increasing molar ratio, the amount and average rate of hydrogen production increased gradually and then reached maximum values of 19.7 mmol and 394 mmol h^{-1} g^{-1}, respectively, for CdS/MoS_2-1. The amount and average rate decreased as the molar ratio continued to increase. The average rates of photocatalytic hydrogen production for mechanically mixed CdS and MoS_2 were also measured. The experimental results of hydrogen production showed a low average rate of 19 mmol h^{-1} g^{-1} for mechanically mixed CdS- and MoS_2-loaded Pt. It was revealed that the interface between CdS and MoS_2 in CdS/MoS_2 contributed to the separation of photogenerated electrons and holes.

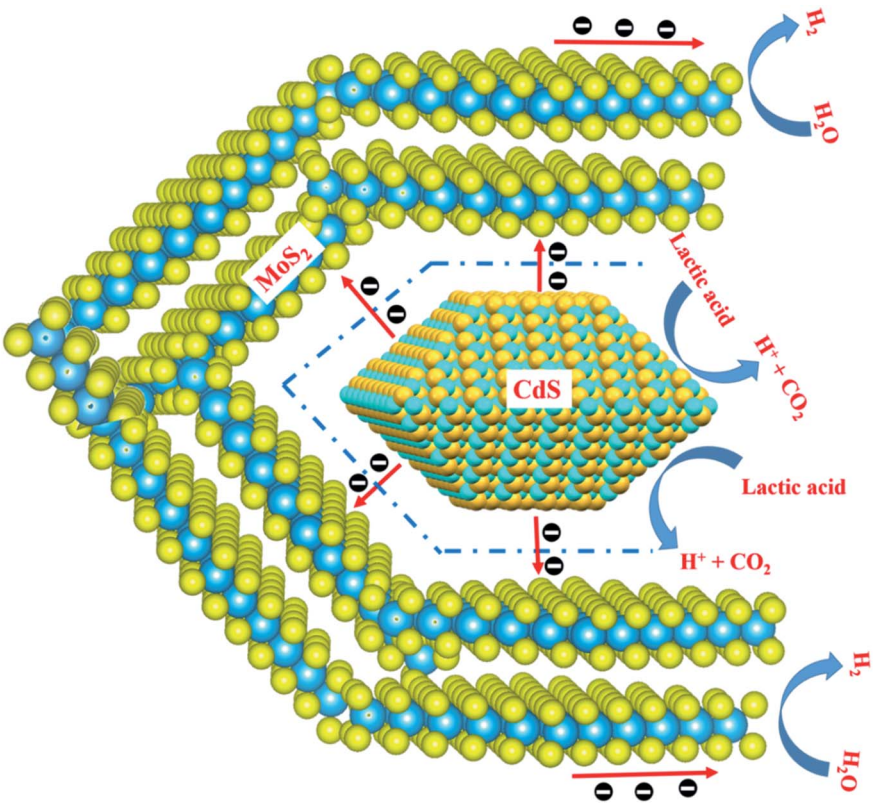

Fig. 9 Schematic diagram of the photogenerated carriers migration between CdS and MoS_2.

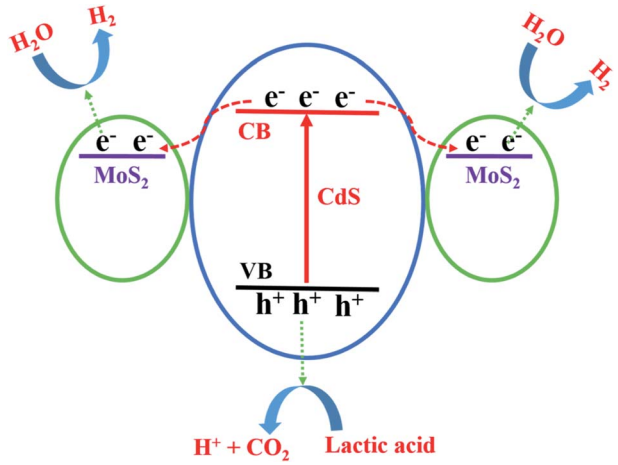

Fig. 10 Migration mechanism of the photogenerated carriers in CdS/MoS_2.

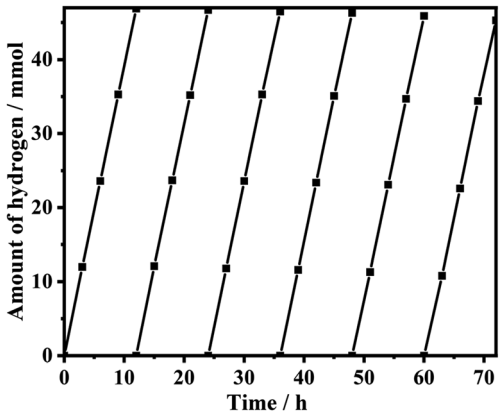

Fig. 12 Long-term photocatalytic hydrogen evolution measurement over CdS/MoS_2-1. Reaction conditions: 0.01 g of catalyst; 200 mL of lactate acid aqueous solution (lactate acid of 10 vol%); 300 W Xe lamp equipped with a cutoff filter (λ > 420 nm).

Through all of the characterization analyses, it was known that the CdS/MoS_2 photocatalyst exhibited a superior efficiency of separation for photogenerated electrons and holes, which was attributed to the special structure of some CdS pyramid structures dispersed in the MoS_2 microsphere structures and surrounded by MoS_2 nanosheets. The different faces of the CdS pyramid structures contacted the surface of the MoS_2 nanosheets to form heterojunctions. Through the heterojunctions, photogenerated electrons could be transferred from the different faces of CdS pyramid structures to different MoS_2 nanosheets, while photogenerated holes remained in CdS pyramid structures. Many highly active dangling bonds existed at the edge of the nanosheets, which could form chemical bonds with H. The ability to bond with H provided the best medium for the convenient adsorption and desorption of H on the surface of the photocatalyst, accelerating the photochemical reaction rate of the photocatalyst interface. Therefore, the photogenerated electrons could continue to migrate to the edge of the MoS_2 nanosheets with highly active dangling bonds and then react with H^+ to form H_2, while the photogenerated holes were consumed by the lactic acid on the surface of the CdS pyramid structures, as shown in Fig. 9. Based on the above analysis, it was revealed that photogenerated electrons migrated from the conduction band of different faces of the CdS pyramid to the conduction band of different MoS_2 nanosheets, while photogenerated holes remained in the CdS pyramid structures, which greatly promoted the separation of photogenerated electrons and holes, improving the photoactivity of the CdS/MoS_2 catalyst, as shown in Fig. 10.

It is known that the photogenerated electrons could be transferred from the CdS to MoS_2 or Pt, while photogenerated holes remained in CdS, resulting in a superior efficiency of separation for photogenerated electrons and holes in the CdS catalyst, and improving the photocatalytic hydrogen production efficiency for CdS catalyst. The photoactivity of CdS was greatly improved by coloaded Pt, mainly because Pt could capture photogenerated electrons from CdS, further promoting the separation of photogenerated carriers. To provide additional evidence for the migration path of the photogenerated electrons between CdS and MoS_2 in the CdS/MoS_2 catalyst, the hydrogen production activity for Pt-loaded CdS/MoS_2-1 was studied, as shown in Fig. 11a. The results showed that the average rate of photocatalytic hydrogen production for CdS/MoS_2-1 was much

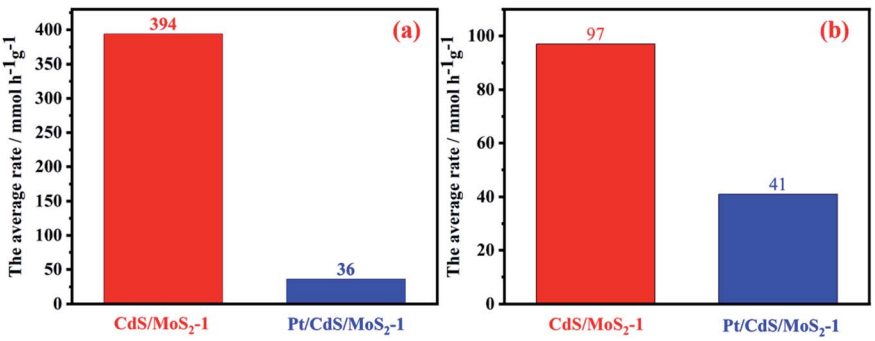

Fig. 11 The average rates of photocatalytic hydrogen production for CdS/MoS_2-1 and Pt loaded CdS/MoS_2-1. Reaction conditions (a): 0.01 g of catalyst; 200 mL of lactate acid aqueous solution (lactate acid of 10 vol%); 300 W Xe lamp equipped with a cutoff filter (λ > 420 nm); reaction conditions (b): the same but substituting 0.25 M Na_2SO_3/0.35 M Na_2S solution for the lactate acid solution.

higher than that of Pt-loaded CdS/MoS_2. It is known that the Pt-loaded CdS catalyst exhibits excellent photoactivity in the sacrificial agent system of Na_2SO_3/Na_2S. To eliminate this effect, the activity of hydrogen production for Pt-loaded CdS/MoS_2-1 in a 0.25 M Na_2SO_3/0.35 M Na_2S solution was studied, as shown in Fig. 11b. The results showed that the average rate of CdS/MoS_2-1 was still higher than that of Pt-loaded CdS/MoS_2-1. According to the above experimental results, photogenerated electrons migrated from the conduction band of CdS to the conduction band of MoS_2. Pt could capture photogenerated electrons of CdS, leading to a decrease in photogenerated electron migration to MoS_2 conduction. This, in turn, resulted in a decrease in the hydrogen production activity for CdS/MoS_2. This finding was consistent with the experimental results.

The stability of CdS/MoS_2-1 in a lactic acid solution was studied, as shown in Fig. 12. CdS/MoS_2-1 exhibited perfect stability, the photoactivity displayed no significant degradation during continuous hydrogen production over nearly 70 h, and the photoactivity of CdS/MoS_2-1 was reduced by only 1.6 mmol after 72 h of photocatalytic reaction.

4. Conclusions

In summary, an irregular CdS pyramid/flower-like MoS_2 microsphere composite photocatalyst was successfully synthesized, achieving a hydrogen evolution rate of 394 mmol g^{-1} h^{-1} with an extremely high apparent quantum yield (AQY = 64.8%) at 420 nm. To our knowledge, this value is the highest efficiency ever reported for MoS_2-modified CdS photocatalysts. Because of the special structure of some CdS pyramid structures dispersed in the MoS_2 microsphere structures and surrounded by MoS_2 nanosheets, the photogenerated electrons migrated from the conduction band of different faces of the CdS pyramid to the conduction band of different MoS_2 nanosheets. Meanwhile, photogenerated holes remained in the CdS pyramid structures, which greatly promoted the separation of photogenerated electrons and holes, improving the photoactivity of the CdS/MoS_2 catalyst. The catalyst also exhibited perfect stability, and the photoactivity displayed no significant degradation during continuous hydrogen production over nearly 70 h. This research has some guiding significance for promoting the study of low-cost and efficient photocatalytic hydrogen production.

Conflicts of interest

There are no conflicts to declare.

References

1 J. Tahereh, M. Ehsan, S. A. Alireza, *et al.*, Photocatalytic water splitting-the untamed dream: A review of recent advances, *Molecules*, 2016, **21**, 900–929.
2 T. M. Su, Q. Shao, Z. Z. Qin, *et al.*, Role of interfaces in two-dimensional photocatalyst for water splitting, *ACS Catal.*, 2018, **8**, 2253–2276.
3 G. Liu, C. Zhen, Y. Y. Kang, *et al.*, Unique physicochemical properties of two-dimensional light absorbers facilitating photocatalysis, *Chem. Soc. Rev.*, 2018, **47**, 6410–6444.
4 Z. Wang, C. Li and K. Domen, Recent developments in heterogeneous photocatalysts for solar-driven overall water splitting, *Chem. Soc. Rev.*, 2018, **10**, 1039–1046.
5 T. Takata and K. Domen, Particulate photocatalysts for water splitting: Recent advances and future prospects, *ACS Energy Lett.*, 2019, **10**, 1021–1048.
6 L. J. Guo, Y. B. Chen, J. Z. Su, *et al.*, Obstacles of solar-powered photocatalytic water splitting for hydrogen production: A perspective from energy flow and mass flow, *Energy*, 2019, **172**, 1079–1086.
7 X. D. Sun, H. W. Huang, Q. Zhao, *et al.*, Thin-layered photocatalysts, *Adv. Funct. Mater.*, 2020, **1002**, 1910005–1910048.
8 Q. Wang and K. Domen, Particulate photocatalysts for light-driven water splitting: mechanisms, challenges, and design strategies, *Chem. Rev.*, 2020, **120**, 919–985.
9 M. C. Liu, L. Z. Wang, L. J. Guo, *et al.*, Twins in $Cd_{1-x}Zn_xS$ solid solution: Highly efficient photocatalyst for hydrogen generation from water, *Energy Environ. Sci.*, 2011, **4**, 1372–1378.
10 M. C. Liu, D. W. Jing, L. J. Guo, *et al.*, Twin-induced one-dimensional homojunctions yield high quantum efficiency for solar hydrogen generation, *Nat. Commun.*, 2013, **4**, 2278–2286.
11 K. He, M. Wang and L. J. Guo, Novel-CdS-nanorod with stacking fault structures: Preparation and properties of visible-light-driven photocatalytic hydrogen production from water, *Chem. Eng. J.*, 2015, **279**, 747–756.
12 K. He and L. J. Guo, The theoretical calculation and analysis of the chemical equilibrium in the synthetic process and its effect on hydrogen production performance for sulfide catalysts, *Int. J. Hydrogen Energy*, 2021, **46**, 6561–6572.
13 B. Li, Y. Si, Q. Fang, *et al.*, Hierarchical self-assembly of well-defned Louver-Like P-doped carbon nitride nanowire arrays with highly efficient hydrogen evolution, *Nano-Micro Lett.*, 2020, **12**, 52–68.
14 X. X. Wang, M. C. Liu, L. J. Guo, *et al.*, Toward facet engineering of CdS nanocrystals and their shape-dependent photocatalytic activities, *J. Phys. Chem. C*, 2015, **119**, 20555–20560.
15 Y. Luo, S. Suzuki, Z. Wang, *et al.*, Construction of spatial charge separation facets on $BaTaO_2N$ crystals by flux growth approach for visible-light-driven H_2 production, *ACS Appl. Mater. Interfaces*, 2019, **11**, 22264–22271.
16 D. Li, R. T. Chen, P. P. Wang, *et al.*, Effect of facet-selective assembly of cocatalyst on $BiVO_4$ photoanode for solar water oxidation, *ChemCatChem*, 2019, **11**, 3763–3769.
17 S. S. Chen, G. J. Ma, Q. Wang, *et al.*, Metal selenide photocatalysts for visible-light-driven Z-scheme pure water splitting, *J. Mater. Chem. A*, 2019, **7**, 7415–7422.
18 H. J. Yan, J. H. Yang, G. J. Ma, *et al.*, Visible-light-driven hydrogen production with extremely high quantum efficiency on Pt-PdS/CdS photocatalyst, *J. Catal.*, 2009, **266**, 165–168.

19 J. H. Yang, H. J. Yan, X. L. Wang, *et al.*, Roles of cocatalysts in Pt-PdS/CdS with exceptionally high quantum efficiency for photocatalytic hydrogen production, *J. Catal.*, 2012, **290**, 151–157.

20 Q. Zuo, T. T. Liu, C. S. Chen, *et al.*, Ultrathin metal–organic framework nanosheets with ultrahigh loading of single Pt atoms for efficient visible-light-driven photocatalytic H_2 evolution, *Angew. Chem.*, 2019, **131**, 10304–10309.

21 M. C. Liu, Y. B. Chen, L. J. Guo, *et al.*, Photocatalytic hydrogen production using twinned nanocrystals and an unanchored NiS_x co-catalyst, *Nat. Energy*, 2016, **1**, 151–159.

22 Z. X. Qin, Y. B. Chen, L. J. Guo, *et al.*, Intergrowth of cocatalysts with host photocatalysts for improved solar-to-hydrogen conversion, *ACS Appl. Mater. Interfaces*, 2015, **8**, 1264–1272.

23 Z. X. Qin, Y. B. Chen, L. J. Guo, *et al.*, Composition-dependent catalytic activities of noble-metal-free NiS/Ni_3S_4 for hydrogen evolution reaction, *J. Phys. Chem. C*, 2016, **120**, 14581–14589.

24 Z. X. Qin, Y. B. Chen, L. J. Guo, *et al.*, A bifunctional NiCoP-based core/shell cocatalyst to promote separate photocatalytic hydrogen and oxygen generation over graphitic carbon nitride, *J. Mater. Chem. A*, 2017, **5**, 19025–19035.

25 K. He and L. J. Guo, NiS modified CdS pyramids with stacking fault structures: Highly efficient and stable photocatalysts for hydrogen production from water, *Int. J. Hydrogen Energy*, 2017, **42**, 23995–24005.

26 X. Y. Xu, F. L. Luo, G. Zhou, *et al.*, Self-assembly optimization of cadmium/molybdenum sulfide hybrids by cation coordination competition toward extraordinarily efficient photocatalytic hydrogen evolution, *J. Mater. Chem. A*, 2018, **6**, 18396–18402.

27 Y. Liu, H. T. Niu, W. Gu, *et al.*, *In situ* construction of hierarchical CdS/MoS_2 microboxes for enhanced visible-light photocatalytic H_2 production, *Chem. Eng. J.*, 2018, **339**, 117–124.

28 M. Chai, M. Q. Xu, C. L. Wang, *et al.*, One-step hydrothermal preparation of MoS_2 loaded on $CdMoO_4$/CdS hybrids for efficient photocatalytic hydrogen evolution, *Catal. Commun.*, 2018, **110**, 10–13.

29 S. A. Darsara, M. Seifi, M. B. Askari, *et al.*, One-step hydrothermal synthesis of MoS_2/CdS nanocomposite and study of structural, photocatalytic, and optical properties of this nanocomposite, *Optik*, 2018, **169**, 249–256.

30 Y. Y. Liu, C. M. Zeng, L. H. Ai, *et al.*, Boosting charge transfer and hydrogen evolution performance of CdS nanocrystals hybridized with MoS_2 nanosheets under visible light irradiation, *Appl. Surf. Sci.*, 2019, **484**, 692–700.

31 D. T. Zhang, T. Y. Xu, M. Y. Cao, *et al.*, Facile band alignment of $C_3N_4/CdS/MoS_2$ sandwich hybrid for efficient charge separation and high photochemical performance under visible-light, *Powder Technol.*, 2019, **351**, 222–228.

32 S. S. Bhata, S. A. Pawarb, D. Potphode, *et al.*, Substantially enhanced photoelectrochemical performance of TiO_2 nanorods/CdS nanocrystals heterojunction photoanode decorated with MoS_2 nanosheets, *Appl. Catal., B*, 2019, **259**, 102–118.

33 H. Lee, D. A. Reddy, D. P. Kumar, *et al.*, Ultra-small cobalt nanocrystals embedded in 2D-MoS_2 nano-sheets as efficient co-catalyst for solar-driven hydrogen production: Study of evolution rate dependence on cobalt nanocrystal size, *Appl. Surf. Sci.*, 2019, **494**, 239–248.

34 X. L. Yin, L. L. Li, D. C. Li, *et al.*, Noble-metal-free $CdS@MoS_2$ core-shell nanoheterostructures for efficient and stabilized visible-light-driven H_2 generation, *Int. J. Hydrogen Energy*, 2019, **44**, 16657–16666.

35 D. A. Reddy, E. H. Kim, M. Gopannagari, *et al.*, Few layered black phosphorus/MoS_2 nanohybrid: A promising co-catalyst for solar driven hydrogen evolution, *Appl. Catal., B*, 2019, **241**, 491–498.

36 T. A. Ho, C. D. Bae, J. Joe, *et al.*, Heterojunction photoanode of atomic-layer-deposited MoS_2 on single-crystalline CdS nanorod arrays, *ACS Appl. Mater. Interfaces*, 2019, **11**, 37586–37594.

37 L. Lin, S. Y. Huang, Y. X. Zhu, *et al.*, Construction of CdS/MoS_2 heterojunction from core–shell MoS_2@Cd-MOF for efficient photocatalytic hydrogen evolution, *Dalton Trans.*, 2019, **48**, 2715–2721.

38 S. B. Patil, B. Kishore, R. Vishwanatha, *et al.*, $CdS@MoS_2$ core–shell nanospheres: a new electrode for lithium ion batteries, *J. Mater. Sci.: Mater. Electron.*, 2019, **30**, 14456–14463.

39 S. R. Kadam, S. W. Gosavi, B. B. Kale, *et al.*, Unique $CdS@MoS_2$ core shell heterostructure for efcient hydrogen generation under natural sunlight, *Sci. Rep.*, 2019, **9**, 12036–12046.

40 S. Jiang, Q. Hu, M. Y. Xu, *et al.*, Crystalline CdS/MoS_2 shape-controlled by a bacterial cellulose scaffold for enhanced photocatalytic hydrogen evolution, *Carbohydr. Polym.*, 2020, **250**, 116909–116919.

41 W. Zhao, J. C. Liu, Z. X. Ding, *et al.*, Optimal synthesis of platinum-free 1D/2D CdS/MoS_2 (CM) heterojunctions with improved photocatalytic hydrogen production performance, *J. Alloys Compd.*, 2020, **813**, 152234–152244.

42 P. X. Li, H. Zhao, X. Y. Yan, *et al.*, Visible-light-driven photocatalytic hydrogen production coupled with selective oxidation of benzyl alcohol over $CdS@MoS_2$ heterostructures, *Sci. China Mater.*, 2020, **63**, 2239–2250.

43 X. N. Liu, J. S. Li and W. T. Yao, $CdS@MoS_2$ hetero-structured nanocomposites are highly effective photo-catalysts for organic dye degradation, *ACS Omega*, 2020, **5**, 27463–27469.